The FreeEOS Code for Calculating the Equation of State for Stellar Interiors IV: The Treatment of the Exchange Effect

Alan W. Irwin

Department of Physics and Astronomy, University of Victoria,
P.O. Box 3055, Victoria, British Columbia, Canada, V8W 3P6
Electronic mail: irwin@beluga.phys.uvic.ca

ABSTRACT

This paper describes how the exchange effect is treated in FreeEOS (http://freeeos.sourceforge.net/), a software package for rapidly calculating the equation of state for physical conditions in stellar interiors. An approximation has been derived as a function of degeneracy and temperature for the exchange effect in the grand canonical partition function representation, a further approximation has been derived for the transformation of that exchange effect into a free-energy representation that can be used by FreeEOS, and the effect of exchange is illustrated for physical conditions appropriate to stellar-interior models.

Subject headings: exchange interaction — approximation of exchange integrals — equation of state — stellar interiors — stellar evolution

1. Introduction

FreeEOS (http://freeeos.sourceforge.net/) is a software package for rapidly calculating the equation of state (hereafter, EOS) for stellar conditions, and a series of papers is being prepared that describe its implementation. Paper I (Irwin 2004a) describes the Fermi-Dirac integral approximations. Paper II (Irwin 2004b) describes the efficient method of solution that delivers thermodynamically consistent results of high numerical quality that are in good agreement with OPAL EOS2001 (Rogers & Nafanov 2002) results for the solar case. Paper III (Irwin 2005) describes the implementation of the Coulomb correction.

The purpose of this fourth paper in the series is to present the implementation of the correction for the exchange effect. This effect depends on the quantum mechanical properties of the total wave function when electrons (or positrons) are exchanged. (Equivalent quantum mechanical effects exist for the ions, but these turn out to be negligible because of the much larger mass of the ions.) Even for the case of no electrostatic repulsion, the anti-symmetrized total wave function of the electrons tends to decrease the spatial overlap of the probability densities of individual electrons. Because of this anti-correlation of the individual electrons, the exchange effect causes the total energy to be decreased in the presence of the electrostatic repulsion, and less pressure is required to confine the

gas to a particular volume for a given temperature. The exchange effect is typically the 3rd most important non-ideal effect for stellar-interior conditions (after pressure-ionization and the Coulomb effect) so an accurate treatment of the effect is important.

The remainder of this paper is organized as follows: Section 2 presents the first-order grand canonical partition function expression that the FreeEOS implementation uses to describe the effect of exchange; Section 3 presents approximation forms for the required exchange integrals; Section 4 describes the least-squares fits for the required exchange integrals; Section 5 shows how the exchange component of the grand canonical partition function result described in Section 2 is transformed to the exchange component of the free energy; Section 6 summarizes the characteristics of the FreeEOS calculations of this paper; while Sections 7, 8, and gives 9 give the results, discussion and conclusions.

2. The Exchange Term in the Grand Canonical Partition Function

The purpose of the present section is to develop the expression for $\ln Z_X$, the change in the natural log of the grand canonical partition function due to first-order exchange. I will develop the transformation of $\ln Z_X$ into the required exchange component of the free energy in Section 5.

For the general case of partially degenerate, semirelativistic electrons and positrons, Kapusta (1989, eq.[5.55]) has given an expression for $\ln Z_X$ that Heckler (1994) has used for determining the importance of the exchange effect under a wide variety of astrophysical conditions. In the limit of no pair production ($-\eta\beta \ll 1$, where $\eta \equiv \mu_e/kT$ with μ_e defined as the chemical potential of the electron and $\beta \equiv kT/(m_e c^2)$) the Kapusta expression (in the SI units that are used throughout this paper) reduces to

$$\ln Z_X(\eta,\beta,V) = \ln Z_X^I(\eta,\beta,V) + \ln Z_X^{II}(\eta,\beta,V); \tag{1}$$

where

$$\ln Z_X^I(\eta,\beta,V) = -\frac{V}{2\pi m_e h^4 \beta}\frac{e^2}{4\pi\epsilon_0}\int \frac{X(p,q)N(\eta,\beta,p)N(\eta,\beta,q)\; d^3p\; d^3q}{[E(p)+m_e c^2][E(q)+m_e c^2]}, \tag{2}$$

$$\ln Z_X^{II}(\eta,\beta,V) = -\frac{4\pi^2 m_e c\beta V}{3h^4}\frac{e^2}{4\pi\epsilon_0}\int \frac{N(\eta,\beta,p)\; d^3p}{E(p)+m_e c^2}, \tag{3}$$

$$N(\eta,\beta,p) = \left[\exp\left(\frac{E(p)}{m_e c^2\beta} - \eta\right) + 1\right]^{-1}, \tag{4}$$

$$E(p) = (m_e^2 c^4 + p^2 c^2)^{1/2} - m_e c^2, \tag{5}$$

and

$$X(p,q) = 1 + \frac{2m_e^2 c^4}{[E(p)-E(q)]^2 - c^2|\vec{p}-\vec{q}|^2}. \tag{6}$$

Note that $-kT \ln Z_X^I(\eta, \beta, V)$ is the same as Ω_x in the notation of the widely referenced exchange treatment of Kovetz, Lamb, & Van Horn (1972, hereafter KLVH). Thus, the present equation (2) corresponds to KLVH, equation (1). Furthermore, KLVH have defined and investigated the exchange integrals J and I which simplify the expression for $\ln Z_X$.

The J integral is defined by

$$J \equiv \beta^2(J^i J^{ii} + J^{iii}); \tag{7}$$

where

$$J^i = \frac{1}{\beta^{1/2}} \int_0^\infty \frac{(u_1 - 1/u_1)\, \mathrm{d}x_1}{\exp(x_1 - \eta) + 1}, \tag{8}$$

$$J^{ii} = \frac{1}{\beta^{1/2}} \int_0^\infty \frac{\exp(x_2 - \eta) \ln u_2\, \mathrm{d}x_2}{[\exp(x_2 - \eta) + 1]^2}, \tag{9}$$

$$J^{iii} = \frac{1}{\beta} \int_0^\infty \int_0^\infty \frac{(u_1 - u_2)(1 - u_1 u_2)}{u_1 u_2} \frac{\ln|(1 - u_1 u_2)/(u_1 - u_2)| \exp(x_2 - \eta)\, \mathrm{d}x_1\, \mathrm{d}x_2}{[\exp(x_1 - \eta) + 1][\exp(x_2 - \eta) + 1]^2}, \tag{10}$$

$$u_1 \equiv 1 + \beta x_1 + \sqrt{2\beta x_1 + \beta^2 x_1^2}, \tag{11}$$

and

$$u_2 \equiv 1 + \beta x_2 + \sqrt{2\beta x_2 + \beta^2 x_2^2} \tag{12}$$

(see KLVH, eq. [43]). The non-relativistic limit of the J integral is

$$J^{\mathrm{NR}} = 2\beta^2 G(\eta), \tag{13}$$

where

$$G(\eta) \equiv \int_0^\infty \int_0^\infty \frac{\ln(x_1^{1/2} + x_2^{1/2}) - \ln|x_1^{1/2} - x_2^{1/2}|}{[\exp(x_1 - \eta) + 1][\exp(x_2 - \eta) + 1]} \mathrm{d}x_1 \mathrm{d}x_2 \equiv \int_{-\infty}^{\eta} [F_{-1/2}(\eta')]^2 d\eta' \tag{14}$$

(see KLVH, eqs. [37] and [38]) with $F_k(\eta) \equiv F_k(\eta, 0)$ and the Fermi-Dirac integral of order k defined by

$$F_k(\eta, \beta) \equiv \int_0^\infty \frac{x^k [1 + (1/2)\beta x]^{1/2} \mathrm{d}x}{\exp(x - \eta) + 1} \tag{15}$$

(see Cox and Giuli 1968, hereafter CG, eq. [24.97]). The equivalence of the two definitions for $G(\eta)$ can be proved by showing the two expressions are identical in the limit of large negative η (see KLVH eq. [40] and CG eq. [24.47]) and then proving the derivatives of the two expressions with respect to η are identical using integration by parts on the derivative of the first expression. The Harwood approximation for $G(\eta)$ (programmed by D. Harwood in the late 60's at Lawrence Livermore and now distributed [see subroutine *f_psi*] as part of FreeEOS) helps to provide a high-quality approximation for J^{NR}.

The I integral is defined by

$$I \equiv K^2, \tag{16}$$

where

$$K \equiv 2\beta^{3/2} F_{1/2}(\eta, \beta) \tag{17}$$

(see KLVH, eq. [42]). The non-relativistic limit of the K integral is

$$K^{\rm NR} \equiv 2\beta^{3/2} F_{1/2}(\eta) = (4/3)\beta^{3/2} F'_{3/2}(\eta). \tag{18}$$

The analytical derivative of the Cody-Thacher (1967) approximation for $F_{3/2}(\eta)$ helps to provide a high-quality approximation for $K^{\rm NR}$.

Using the above definitions of J and K, equation (2) reduces to

$$\ln Z_X^I(\eta, \beta, V) = \frac{4\pi m_e^3 c^2 V}{h^4 \beta} \frac{e^2}{4\pi\epsilon_0} (J - K^2) \tag{19}$$

(see KLVH eq. [6a]), equation (3) reduces to

$$\ln Z_X^{II}(\eta, \beta, V) = -\frac{2^{3/2}\pi^2}{3} \frac{4\pi m_e^3 c^2 V}{h^4 \beta} \frac{e^2}{4\pi\epsilon_0} \beta^2 K, \tag{20}$$

and equation (1) reduces to

$$\ln Z_X(\eta, \beta, V) = \frac{4\pi m_e^3 c^2 V}{h^4 \beta} \frac{e^2}{4\pi\epsilon_0} \left(J - K^2 - \frac{2^{3/2}\pi^2}{3} \beta^2 K \right). \tag{21}$$

Equation (21) is the fundamental expression used for the exchange treatment in the FreeEOS implementation, and it relates to other exchange expressions as follows. This equation is a special case (with pair production ignored) of equation (5.55) from Kapusta (1989). If the term that is proportional to $\beta^2 K$ is dropped, then equation (21) is equivalent to the KLVH expression which is used both by the Stolzmann & Blöcker (1996) EOS (with the linear-inversion approximation given by eq. (50) below) and the OPAL (Rogers & Nayfonov 2002) EOS. Finally, the linear-inversion approximation of the non-relativistic limit of equation (21) is equivalent to equation (17) of DeWitt (1969).

3. Approximation Forms for the Exchange Integrals

The purpose of the present section is to develop approximation forms for the J and K exchange integrals that are defined by equations (7) and (17) and which appear in equation (21). Since EFF-style approximations for Fermi-Dirac integrals have proved to give excellent results even in low-order (see Paper I and Eggleton, Faulkner, and Flannery 1973, hereafter EFF), I adapt that approximation method to the present case where the components of the J integral (eqs. [8], [9], and [10]) have an exponential cutoff in the x_1 and x_2 integrands like that occurring for Fermi-Dirac integrals, and the K integral (eq. [17]) is already proportional to a Fermi-Dirac integral. As in

EFF and Paper I, the approximations are expressed as a function of the f and g fitting parameters defined implicitly by

$$\eta \equiv 2\sqrt{1+f} + \ln \frac{\sqrt{1+f}-1}{\sqrt{1+f}+1} \tag{22}$$

and

$$g \equiv \beta\sqrt{1+f} \tag{23}$$

with approximate expansions

$$f(\eta) \simeq \exp(\eta) \sum_{m=0} f_m^{(1)} \exp(m\eta) \ \ (\eta \ll -1), \tag{24}$$

$$f(\eta) \simeq \eta^2 \sum_{m=0} f_m^{(2)} \eta^{-2m} \ \ (\eta \gg 1), \tag{25}$$

$$g(\eta,\beta) \simeq \beta \sum_{n=0} g_n^{(1)} \exp(n\eta) \ \ (\eta \ll -1), \tag{26}$$

and

$$g(\eta,\beta) \simeq \eta\beta \sum_{n=0} g_n^{(2)} \eta^{-2n} \ \ (\eta \gg 1) \tag{27}$$

(see EFF eqs.[7] through [10] and note that the EFF T parameter is the same as the present β). These fitting parameters help to achieve the correct form of results for the approximations to the J and K integrals in the four limits ($\eta \ll -1, \beta \ll 1$); ($\eta \gg 1, \eta\beta \ll 1$); ($\eta \ll -1, \beta \gg 1$); and ($\eta \gg 1, \eta\beta \gg 1$).

3.1. Approximation form for the J integral

There exist the following general form of expansions (some convergent some asymptotic) in four different limits for J:

$$J \simeq J^{\rm NR} + \beta^3 \exp(2\eta) \sum_{m,n=0} j_{m,n}^{(1)} \exp(m\eta)\beta^n \ \ (\eta \ll -1, \beta \ll 1) \tag{28}$$

(see eq. [13], KLVH eq. [36], and CG eq. [24.47]);

$$J \simeq J^{\rm NR} + (\eta\beta)^3 \sum_{m,n=0} j_{m,n}^{(2)} \eta^{-2m} (\eta\beta)^n \ \ (\eta \gg 1, \eta\beta \ll 1) \tag{29}$$

(see eq. [13], KLVH eq. [36], and CG eq. [24.38]);

$$J \simeq \beta^2 \exp(\eta) \sum_{m,n=0} [j_{m,n}^{(3)} + j_{m,n}^{\prime(3)} \ln\beta - j_{m,n}^{\prime\prime(3)} \beta^{-2} \ln^2\beta] \exp(m\eta)\beta^{-n} \ \ (\eta \ll -1, \beta \gg 1) \tag{30}$$

(see KLVH eqs. [25b] and [30] and CG eq. [24.263]); and

$$\begin{aligned} J \ \ \simeq \ \ & (\eta\beta)^2 \sum_{m,n=0} [j_{m,n}^{(4)} + j_{m,n}^{\prime(4)} \ln(\eta\beta) - j_{m,n}^{\prime\prime(4)} \eta^{-2} \ln\eta - \\ & j_{m,n}^{\prime\prime\prime(4)} (\eta\beta)^{-2} \ln^2(\eta\beta)] \eta^{-2m} (\eta\beta)^{-n} \ \ (\eta \gg 1, \eta\beta \gg 1) \end{aligned} \tag{31}$$

(see KLVH eqs. [12], [17], [20], and [22]); where $j^{(k)}_{m,n}$, $j^{\prime(k)}_{m,n}$, $j^{\prime\prime(k)}_{m,n}$ and $j^{\prime\prime\prime(k)}_{m,n}$ are numerical coefficients. (Note that the KLVH β parameter is the inverse of the present [and CG] β.)

I have adopted the following approximation formula for the J integral:

$$J \simeq \frac{J^{\rm NR}}{(1+g)^{N+1}} + \frac{f^2}{(1+f)^2}\frac{g^3}{1+g}\left[\frac{\sum_{m=0}^{M}\sum_{n=0}^{N}\widehat{J}_{m,n}f^m g^n}{(1+f)^M(1+g)^N} + \ln(1+g)\frac{\sum_{m=0}^{M'}\sum_{n=0}^{N'}\widehat{J'}_{m,n}f^m g^n}{(1+f)^{M'}(1+g)^{N'}} - \frac{\ln(1+f)}{(1+f)}\frac{\sum_{m=0}^{M''}\sum_{n=0}^{N''}\widehat{J''}_{m,n}f^m g^n}{(1+f)^{M''}(1+g)^{N''}} - \frac{\ln^2(1+g)}{(1+g)^2}\frac{\sum_{m=0}^{M'''}\sum_{n=0}^{N'''}\widehat{J'''}_{m,n}f^m g^n}{(1+f)^{M'''}(1+g)^{N'''}}\right]. \quad (32)$$

If the limiting forms for f and g given by equations (24) through (27) are taken into account, then this approximation formula reduces to the form of equations (28) through (31) in the appropriate limits. Following Paper I, the $J^{\rm NR}$ term has been kept separate in this approximation formula because a high-quality approximation (see Sect. 2) exists for it which greatly reduces the fitting errors of this approximation form in the important non-relativistic limit. The numerical coefficients $\widehat{J}_{m,n}$, $\widehat{J'}_{m,n}$, $\widehat{J''}_{m,n}$ and $\widehat{J'''}_{m,n}$ must be determined by fitting precise values of J (see, e.g., Sect. 4).

3.2. Approximation form for the K integral

There exist the following general form of expansions (some convergent some asymptotic) for $K \equiv 2\beta^{3/2}F_{1/2}(\eta,\beta)$:

$$K \simeq K^{\rm NR} + \beta^{5/2}\exp(\eta)\sum_{m,n=0} k^{(1)}_{m,n}\exp(m\eta)\beta^n \quad (\eta \ll -1, \beta \ll 1) \quad (33)$$

(see eq. (18) and CG eqs. [24.47] and [24.289]);

$$K \simeq K^{\rm NR} + (\eta\beta)^{5/2}\sum_{m,n=0} k^{(2)}_{m,n}\eta^{-2m}(\eta\beta)^n \quad (\eta \gg 1, \eta\beta \ll 1) \quad (34)$$

(see eq. (18) and CG eqs. [24.38] and [24.289]);

$$K \simeq \beta^2\exp(\eta)\sum_{m,n=0} [k^{(3)}_{m,n} - k^{\prime(3)}_{m,n}\beta^{-2}\ln\beta]\exp(m\eta)\beta^{-n} \quad (\eta \ll -1, \beta \gg 1) \quad (35)$$

(see CG eqs. [24.236] and [24.265]); and

$$K \simeq (\eta\beta)^2\sum_{m,n=0} [k^{(4)}_{m,n} - k^{\prime(4)}_{m,n}(\eta\beta)^{-2}\ln(\eta\beta)]\eta^{-2m}(\eta\beta)^{-n} \quad (\eta \gg 1, \eta\beta \gg 1) \quad (36)$$

(see CG eqs. [24.179] and [24.197]); where $k^{(k)}_{m,n}$ and $k^{\prime(k)}_{m,n}$ are numerical coefficients.

I have adopted the following approximation formula for the K integral:

$$K \simeq \frac{K^{\rm NR}}{(1+g)^{N+1/2}} + \frac{f}{1+f}\frac{g^{5/2}}{(1+g)^{1/2}}\left[\frac{\sum_{m=0}^{M}\sum_{n=0}^{N}\widehat{K}_{m,n}f^m g^n}{(1+f)^M(1+g)^N} - \frac{\ln(1+g)}{(1+g)^2}\frac{\sum_{m=0}^{M'}\sum_{n=0}^{N'}\widehat{K'}_{m,n}f^m g^n}{(1+f)^{M'}(1+g)^{N'}}\right]. \quad (37)$$

If the limiting forms for f and g given by equations (24) through (27) are taken into account, then this approximation formula reduces to the form of equations (33) through (36) in the appropriate limits. Following Paper I, the $K^{\rm NR}$ term has been kept separate in this approximation formula because a high-quality approximation (see Sect. 2) exists for it which greatly reduces the fitting errors of this approximation form in the important non-relativistic limit. The numerical coefficients $\widehat{K}_{m,n}$ and $\widehat{K'}_{m,n}$ must be determined by fitting precise values of K (see, e.g., Sect. 4).

4. Least-Squares Fitting Procedure

The least-squares fitting procedure used to determine approximations for the J and K integrals follows the method used in Paper I. The least-squares implementation used a singular-value decomposition technique based on the LAPACK *dgesdd* routine (see Anderson, et al. 1999). The inverses of the smallest singular values were automatically edited to zero (see discussion in Chapter 14.3 of Press et al, 1986) in order to assure a condition number that exceeded 10^{-10} (i.e., to assure at least a nominal 6 significant digits in the derived fitting coefficients for these double-precision [64-bit floating point] results). All fits employed a 61×61 equally spaced grid of points over the ranges $-15 \le \ln f \le 15$ and $-15 \le \ln g \le 15$. As in Paper I all numerical integrations required to determine the values being fitted were performed with a 4-point Gauss quadrature method that locally bisected the integration range a sufficient number of times to assure relative errors in the results that were smaller than of 1 part in 10^9.

4.1. The fit of the J integral

I determined the $\widehat{J}_{m,n}$, $\widehat{J'}_{m,n}$, $\widehat{J''}_{m,n}$ and $\widehat{J'''}_{m,n}$ coefficients of equation (32) with the least-squares method described above for a number of different orders. The fitted J integral values were determined from equation (7) with J^i, J^{ii}, and J^{iii} calculated by numerical integration of equations (8), (9), and (10). In the case of J^{iii}, the transformation,

$$\int_0^\infty\int_0^\infty f(x_1,x_2)\mathrm{d}x_1\mathrm{d}x_2 = \int_0^\infty\int_0^{x_2}[f(x_1,x_2)+f(x_2,x_1)]\mathrm{d}x_1\mathrm{d}x_2 \quad (38)$$

was used to avoid the occurrence of singularities of the derivative of the integrand in the middle of the integration range. The $J^{\rm NR}$ values were determined from a high-quality approximation (see Sect. 2).

Following Paper I, I adopted a fitting weight of $\min(10^4 J^{-2}, [J - J^{\rm NR}]^{-2})$. For large g, $J^{\rm NR}$ is negligible relative to J, and this weight approaches J^{-2} which is the weight that if uniformly applied would make the present linear least squares fit of J largely equivalent to an unweighted non-linear fit of $\ln J$. For small g, $(J - J^{\rm NR})^{-2}$ becomes quite large (because the relative differences between the high-quality approximation used to calculate $J^{\rm NR}$ and the precise numerical integration used to calculate J are quite small), and the weight reduces to the limiting $10^4 J^{-2}$ value. The factor of 10^4 used in this limiting value is a good compromise that helps to reduce the residuals in the important low-g region without substantially increasing the residuals in the high-g region.

4.2. The fit of the K integral

I determined the $\widehat{K}_{m,n}$ and $\widehat{K'}_{m,n}$ coefficients of equation (37) with the least-squares method described above. The fitted K integral values were determined from equation (17) with $F_{1/2}(\eta, \beta)$ calculated by numerical integration of equation (15). The $K^{\rm NR}$ values were determined from a high-quality approximation (see Sect. 2). Following what was done for the fit of the J integral, I adopted a fitting weight of $\min(10^4 K^{-2}, [K - K^{\rm NR}]^{-2})$.

5. The Exchange Transformation

The purpose of the present section is to develop an approximation for the transformation of $\ln Z_X$, the first-order exchange term in the natural log of the grand canonical partition function (see eq. [21]), into the corresponding free-energy form. This transformation is necessary for any free-energy based EOS such as FreeEOS, but is obviously not required for any EOS (such as OPAL) that is based on the grand canonical partition function.

The free energy, F, and grand canonical partition function, Z, are related by the definitions,

$$F(\vec{N}, T, V) \equiv \vec{\mu} \cdot \vec{N} - kT \ln Z(\vec{\mu}, T, V) \tag{39}$$

and

$$N_\sigma(\vec{\mu}, T, V) \equiv kT \frac{\partial \ln Z(\vec{\mu}, T, V)}{\partial \mu_\sigma}; \tag{40}$$

where σ ranges over all species, $\vec{N}$ (with components given by eq. [40]) is the vector of numbers of each kind of particle in the volume, V, and $\vec{\mu}$ is the vector of chemical potentials for each kind of particle. Definitions (39) and (40) are completely general. Furthermore, in this section I use the notation that zero subscripts denote quantities where the exchange effect is dropped. Thus, recalling that $\eta = \mu_e/kT$ and $\beta = kT/(m_e c^2)$,

$$\ln Z(\vec{\mu}, T, V) \equiv \ln Z_0(\vec{\mu}, T, V) + \ln Z_X(\eta, T, V) \tag{41}$$

and

$$F(\vec{N}, T, V) \equiv F_0(\vec{N}, T, V) + F_X(\vec{N}, T, V), \tag{42}$$

where $\ln Z_X$ is determined from equation (21), and F_X is the corresponding exchange term in the free-energy model. Note, the independent variables of the free-energy must be identical with and without exchange. Therefore, $\vec{N} = \vec{N_0}$ or

$$N_\sigma(\vec{\mu}, T, V) \equiv kT \frac{\partial \ln Z_0(\vec{\mu}, T, V)}{\partial \mu_\sigma} + \frac{\partial \ln Z_X(\eta, \beta, V)}{\partial \eta} = kT \frac{\partial \ln Z_0(\vec{\mu_0}, T, V)}{\partial \mu_\sigma} \equiv N_\sigma(\vec{\mu_0}, T, V). \quad (43)$$

The preceding equations imply

$$F_X(\vec{N}, T, V) = (\vec{\mu} - \vec{\mu_0}) \cdot \vec{N} - kT[\ln Z_0(\vec{\mu}, T, V) - \ln Z_0(\vec{\mu_0}, T, V) + \ln Z_X(\eta, \beta, V)]. \quad (44)$$

Equations (43) and (44) give the transformation between $\ln Z_X$ and F_X in the general case. Since exact solution of these equations would be computationally expensive, the FreeEOS implementation employs an approximate solution of these equations based on the assumption that only the ideal and exchange components of the free energy depend on N_e, the number of free electrons in V. Under these conditions the electronic part of $kT \ln Z$ separates and is given by

$$\ln Z_e(\eta, \beta, V) = \ln Z_{0e}(\eta, \beta, V) + \ln Z_X(\eta, \beta, V), \quad (45)$$

where

$$\frac{kT}{V} \ln Z_{0e}(\eta, \beta, V) \equiv P_{0e}(\eta, \beta) \equiv \frac{16\pi\sqrt{2}}{3h^3} m_e^4 c^5 \beta^{5/2} [F_{3/2}(\eta, \beta) + (1/2)\beta F_{5/2}(\eta, \beta)] \quad (46)$$

(CG, eq. [24.99]). Furthermore, equations (43) and (44) reduce to

$$n_e(\eta, \beta) \equiv n_{0e}(\eta, \beta) + \frac{1}{V} \frac{\partial \ln Z_X(\eta, \beta, V)}{\partial \eta} = n_{0e}(\eta_0, \beta) \quad (47)$$

and

$$F_X(N_e, T, V) = (\eta - \eta_0) n_{0e}(\eta_0, \beta) kTV - [P_{0e}(\eta, \beta) - P_{0e}(\eta_0, \beta)]V - kT \ln Z_X(\eta, T, V), \quad (48)$$

where $N_e/V \equiv n_e(\eta, \beta)$, and

$$N_{0e}/V \equiv n_{0e}(\eta, \beta) \equiv \frac{1}{kT} \frac{\partial P_{0e}(\eta, \beta)}{\partial \eta} = \frac{8\pi\sqrt{2}}{h^3} m_e^3 c^3 \beta^{3/2} [F_{1/2}(\eta, \beta) + \beta F_{3/2}(\eta, \beta)] \quad (49)$$

(CG, eq. [24.98]). (Note the usual notation is to drop the "0" subscript from P_{0e} and n_{0e}, but this subscript is used for the special notation of this section to emphasize the relationship between these quantities and $\ln Z_{0e}$ and to distinguish n_e [which is related to $\ln Z_e$] from n_{0e}.)

The solution of equations (47) and (48) is straightforward. The FreeEOS implementation employs approximations for the J and K integrals (eqs. [32] and [37]) and thermodynamically consistent approximations for P_{0e} and n_{0e} (Paper I). These approximations are expressed in terms of the convenient fitting parameters f and g that are (implicitly) defined by equations (22) and (23). For the FreeEOS implementation, f_0 and g_0 are readily available since $\ln f_0$ and $\ln T$ are the

independent variables in one mode of the FreeEOS calculation (or in other modes are available at each stage of an outer iteration to determine $\ln f_0$ as a function of either $\ln \rho$ or $\ln P$, see Paper II). Equation (47) is transformed to a form implicitly relating $\ln f$ to $\ln f_0$ and Newton-Raphson iteration quickly and reliably determines $\ln f$ starting with the initial approximation that $\ln f \approx \ln f_0$. F_X then follows directly from equation (48). Note, these calculations and the associated correction to the equilibrium constants given by equation (35) of Paper II are independent of auxiliary variables and can therefore be calculated outside the auxiliary variable loop (see Paper II) saving substantial computer time. Also, all partial derivatives of the exchange transformation calculation are implemented in a consistent way so that thermodynamic consistency in the EOS results is preserved to the order of one part in 10^{11} or better (see Fig. 3 of Paper II).

The current approximation for transforming $\ln Z_X$ to F_X is asymptotically correct for low densities which normally correlate with low degeneracy. For those conditions, *all* non-ideal effects can be considered small perturbations and equation (44) can be replaced by the lowest-order surviving term of its Taylor-series expansion in $\vec{\mu}$,

$$F_X^{\rm linear}(N_e, T, V) \equiv -kT \ln Z_X(\eta_0 = \mu_{0e}/kT, \beta, V). \tag{50}$$

For these same conditions, the first surviving term of the Taylor-series expansion of equation (48) in η also yields the same result.

Equation (50) corresponds to the linear-inversion approximation discussed by Perrot & Dharmawardana (1984). This approximation is used implicitly by Saumon, Chabrier, and Van Horn (1995), Stolzmann & Blöcker (1996), and presumably other free-energy based equations of state that include the exchange effect. Although I have implemented this linear inversion approximation as an option for FreeEOS to help emulate other free-energy based equations of state, I recommend instead the FreeEOS option (which is used automatically as part of the EOS1 option suite) of using the numerical solution of equations (47) and (48) to transform $\ln Z_X$ to F_X. The reason for this recommendation is because the exchange and other non-ideal effects are *not* small perturbations of the EOS for extreme lower-main-sequence conditions (see Sect. 7) in contradiction with the assumption used to derive the linear inversion approximation.

The recommended FreeEOS pressure-ionization treatment uses the occupation probability formulation of Mihalas, Däppen, & Hummer (1988) (with modified interaction radii to fit the OPAL results) which is completely independent of N_e. For large degeneracy the recommended Coulomb treatment (see Paper III) is also independent of N_e. Thus, for these conditions the assumption underlying the derivation of equations (47) and (48) are satisfied, and the recommended option of solving these approximate equations to transform $\ln Z_X$ to F_X should therefore yield asymptotically correct results for large degeneracy.

6. The FreeEOS Equation of State

Some of the following results require EOS calculations which are supplied by the FreeEOS code which has been made publically available at http://freeeos.sourceforge.net/ under the GNU General Public License (GPL). A full description of the FreeEOS code is still in preparation so I will only summarize its principal characteristics here.

The EOS is calculated using an equilibrium-constant approach to minimize the Helmholtz free-energy (Paper II). For realistic abundance mixtures, this approach greatly reduces the number of linear equations that must be solved per iteration so that the solution can be rapidly obtained. This speed makes it practical to call the EOS directly from the stellar-interior code without introducing the errors associated with interpolating EOS tables (Dorman, Irwin, & Pedersen 1991). All calculations are done in double precision (64-bit floating point), and all required partial derivatives are analytically derived and implemented rather than calculated with numerical differences. This approach gives numerical solutions of high quality with thermodynamic consistency which is typically better than 11 decimal digits. Intercomparison of results on different floating-point platforms also confirms there are typically 11 decimal digits of numerical precision or better in the FreeEOS results.

The recommended "EOS1" option suite of FreeEOS includes the following components: arbitrarily relativistic and degenerate free electrons (Paper I); excited electronic states; a Planck-Larkin occupation probability (Rogers 1986); a complete complement of ro-vibrational energy levels for the ground electronic state of H_2 (Irwin 1987) and H_2^+; a pressure-ionization occupation probability formulation similar to that of Mihalas, Däppen, & Hummer (1988); the exchange effect for arbitrarily relativistic and degenerate electrons (see details below); and the Coulomb effect which is treated with the Debye-Hückel approximation in the weak coupling limit that is smoothly joined to a good approximation to liquid multi-component plasma results in the strong-coupling limit (Paper III). The limits of the Coulomb join region and the size of the interaction radii that characterize the pressure-ionization occupation probability are adjusted to fit the OPAL EOS tables distributed at ftp://www-phys.llnl.gov/pub/opal/eos/. In particular, the EOS1 option suite of FreeEOS provides an excellent fit of OPAL results for solar conditions (Paper II).

The 'EOS1" option suite for exchange employs second-order (see Sect. 7) approximations for the J and K integrals in equation (21) to determine $\ln Z_X$, and uses a good approximation (eqs. [47] and [48]) to the non-linear transformation between $\ln Z_X$ and F_X. Other FreeEOS exchange options investigated in this paper are to drop exchange altogether; use higher-order fits to the J and K integrals; use series approximations (see details below) for the J and K integrals; use the non-relativistic limit of equation (21),

$$\ln Z_X(\eta, \beta, V) \approx \frac{4\pi m_e^3 c^2 V}{h^4 \beta} \frac{e^2}{4\pi\epsilon_0} \left(J^{\rm NR}\right); \tag{51}$$

or use the linear inversion approximation (eq. [50]) to transform $\ln Z_X$ to F_X.

FreeEOS implements the option of approximating J and K by series as follows. For $\eta < \eta_{\rm lim} \equiv \max(3, 1/[2\beta])$, J is approximated by the first three terms of KLVH equation (36), and K is approximated by the first two terms of CG equation (24.289). For $\eta > \eta_{\rm lim}$, J is approximated by KLVH equation (12), and K is approximated by CG equation (24.179). The A_1 and A_2 coefficients used in KLVH equation (12) are defined by

$$A_1 \equiv \int_0^\infty \frac{t \ln t}{\exp(t) + 1} dt = 0.4490427560 \tag{52}$$

and

$$A_2 \equiv \int_0^\infty \int_0^\infty \ln \left| \frac{s+t}{s-t} \right| \frac{ds}{\exp(s)+1} \frac{dt}{\exp(t)+1} = 0.5047526561, \tag{53}$$

where the numerical values on the right hand sides of these equations are derived by numerical integration using the technique described in Section 4. These values provide substantially more precision than the KLVH values of A_1 and A_2 (see their eqs. [21] and [23]). Note there is also an error in the sign of the KLVH A_2 value which the present value corrects.

7. Results

7.1. Results in f and g

To give the results that are plotted as a function of the degeneracy parameter f (eq. [22]) and the relativity parameter g (eq. [23]) some context, Figure 1 compares the loci of several stellar-interior models of solar metallicity as a function of f and g. The border between non-degenerate and degenerate conditions occurs at $\log f \approx 0$, and the border between non-relativistic and relativistic conditions occurs at $\log g \approx 0$. Thus, this figure illustrates the well-known results that main-sequence models are non-relativistic, extreme lower-main-sequence model cores are degenerate, red-giant model cores are degenerate and just beginning to be significantly affected by relativistic effects, and there are substantial decreases of both degeneracy and relativistic effects caused by the core helium flash that drives the large changes between the red-giant-tip model and the clump-giant model.

Figure 2 compares results for the $J^{\rm NR}$ integral calculated with equation (13) and precise numerical integration of the non-relativistic limit of the J integral. The maximum relative differences are $10^{-6.4}$ which reflects the maximum relative errors of the Harwood approximation for $G(\eta)$.

Figure 3 compares results for the $K^{\rm NR}$ integral calculated with equation (18) and precise numerical integration of the non-relativistic limit of the K integral. The maximum relative differences are $10^{-7.0}$ which reflects the maximum relative errors of the analytical derivative of the Cody-Thacher approximation for $F_{3/2}(\eta)$.

Figure 4 compares series (see Sect. 6) and precise numerical-integration results for the J and K integrals. For non-degenerate, relativistic conditions, the series are obviously far from their

region of validity; the J series results are incorrect both in sign and order of magnitude and the K series results are incorrect in order of magnitude. Furthermore, there are discontinuities between the two series results employed for each integral. These discontinuities appear on the figures near $\log g = 0$ for $\log f > 1$ and $\log f = 1$ for $\log g > 0$ corresponding to the locus of points where $\eta = \eta_{\rm lim} \equiv \max(3, 1/[2\beta])$. On the other hand, the series results are accurate for the cases for which they are designed; i.e., the non-relativistic case and the degenerate case (so long as the sign of the KLVH value of A_2 is corrected, see Sect. 6). In the non-relativistic limit the errors of the J-series results are dominated by the errors (see Fig. 2) in the Harwood approximation for $G(\eta)$, and the errors in the K-series results are dominated by the errors (see Fig. 3) in the analytical derivative of the Cody-Thacher approximation for $F_{3/2}(\eta)$.

Tables 1 through 6 show coefficients of approximations (eqs. [32] and [37]) for the J and K integrals. These coefficients were derived using the least-squares procedure described in Section 4. The orders of these fits were chosen to reduce the number of coefficients required to achieve a given relative accuracy. For example, the terms proportional to $\ln^2(1+g)$ in equation (32) were completely dropped and the terms proportional to $\ln(1+g)$ in equation (37) were treated in low order without significantly compromising the maximum relative errors of the fits. Figure 5 compares these approximations for the J and K integrals with precise numerical-integration results. These fits for the J and K integrals show good accuracy at low order and the maximum relative errors decrease roughly by an order of magnitude each time the order is increased by 2 units. Because the design of the fitting functions takes advantage of the availability of high-quality approximations for the leading terms of the non-relativistic series, the errors of the J and K approximations are small in the non-relativistic limit and identical to the corresponding errors in the J and K series. Furthermore, the J and K approximations give reasonable errors for all f and g conditions and do not have the discontinuities that are present for the series results for J and K.

7.2. Results in ρ and T

To give the results that are plotted as a function of density ρ and temperature T some context, Figure 6 compares EOS quantities and the loci of several stellar interior models on the density-temperature plane for solar metallicity. The high-density, low-temperature calculation limit indicated in the figure is defined by

$$\log \rho_{\rm lim} = \log \rho_5 + (3/2)\log(T/10^5) \tag{54}$$

for $\log T < 6$ and continued by the $\log T = 6$ isotherm. The limit parameter of $\log \rho_5 = 3.3$ is used for this figure to avoid regions where FreeEOS calculations currently do not converge. This calculation limit roughly corresponds to a 0.1-$M_\odot$ model and can also be viewed as the approximate limit of validity for FreeEOS calculations (see further discussion in Paper II). This same $\log \rho_5$ limit parameter is also used for all other ρ, T figures in this paper.

Figure 7 shows the changes in pressure P and first adiabatic exponent Γ_1 caused by large-scale

changes in the way that exchange is treated in FreeEOS. The effect of the exchange interaction itself are substantial (changes larger than 0.1 in $\ln P$ and Γ_1) for the low temperatures and high densities that occur in the envelopes of extreme lower-main-sequence stars. The errors in the linear inversion approximation for the exchange transformation are also substantial for the same conditions. The errors in EOS results for the non-relativistic approximation for exchange are small; the maximum EOS errors of this approximation are $10^{-2.9}$ for $\ln P$ and $10^{-3.7}$ for Γ_1.

Figure 8 shows Γ_1 and the same differences as in Figure 7 for the locus of points in a (fixed) solar model. The solar effect of the exchange interaction is small but still significant (in light of the precise acoustical frequency inversion data available for the sun, Basu et al. 2003). The errors of the linear inversion approximation for the exchange transformation and the errors of the non-relativistic approximation for exchange are both negligible in the solar case.

Figure 9 shows the changes in pressure P and first adiabatic exponent Γ_1 caused by changes in the way that the J and K exchange integrals are approximated. The EOS errors caused by the series approximations to J and K are small although the expected (see Fig. 4) discontinuity in the results near the onset of relativistic degeneracy is apparent. The EOS errors caused by the recommended second-order fit of J and K are negligible.

8. Discussion

Both the series approximations (Sect. 6) and the fits to the J and K exchange integrals (eqs. [32] and [37] and Tables 1 through 6) have errors which are ideally distributed for EOS calculations. The series and fits have negligible errors in the non-relativistic limit (Figs. 4 and 5) right where the EOS effects of exchange are the strongest (Fig. 7). The EOS effects of exchange drop off rapidly with increasing relativity which has two important effects. (1) The maximum effects of relativistic exchange on the EOS barely exceeds 10^{-3}. Since the term proportional to $\beta^2 K$ in equation (21) is part of this relativistic exchange, this means the EOS differences between the Kapusta exchange formulation (which includes this term) and the KLVH exchange formulation (which drops this term) should be minor. (2) The errors in both the series and fit results to the J and K integrals for relativistic conditions propagate only weakly to the relativistic EOS results, and the associated maximum errors in the EOS results are negligible as a result (Fig. 9). Thus, the exchange series has been used as the basis of the exchange treatment for version 1.4.0 of FreeEOS and all previous versions. The actual motivation for upgrading from the series to the lowest-order exchange fit results for version 1.5.0 of FreeEOS was the removal of the small discontinuity in the series treatment which sometimes caused trouble in the final stages of the Newton-Raphson iterations used in FreeEOS. The actual difference in results (not illustrated) between version 1.4.0 and 1.5.0 of FreeEOS are negligible. Furthermore, since the EOS errors associated with this lowest-order fit are already negligible from today's perspective, there is no benefit to using the higher-order exchange integral approximations at the present time. Thus, these higher-order approximations are reserved for possible future need where precision requirements might be higher than the present.

One uncertainty in all free-energy treatments of exchange is the method used to transform from $\ln Z_X$ in the grand canonical partition function to F_X in the free-energy. The linear inversion approximation (eq. [50]) evidently has large errors (Fig. 7) for the conditions in the envelopes of extreme lower-main-sequence models so I do not recommend it in general although it does give reliable results for the solar case (Fig. 8). Another alternative is to numerically calculate the exchange transformation using the approximations given by equations (47) and (48). This approximate numerical transformation gives a smooth transition between asymptotically correct results for low degeneracy and asymptotically correct results for high degeneracy (Sect. 5). Preliminary comparisons with detailed OPAL calculations (which are based on the grand canonical partition function and which are thus not subject to this transformation uncertainty) indicate the approximate numerical transformation also gives reasonably reliable results at intermediate degeneracy. Accordingly, the option to use this transformation has been part of the EOS1 option suite for all FreeEOS versions.

9. Conclusions

This paper has presented the implementation of the exchange effect for FreeEOS, a software library which is suitable for calculating the EOS for stellar-interior conditions. This implementation is based on the equation (21) for the exchange effect in the grand canonical partition function. The J and K integrals that occur in that equation have been approximated by the fits described by equations 32 and 37 and Tables 1 through 6. As of version 1.5.0 of FreeEOS, the EOS1 option suite employs the second-order version of those fits. The associated EOS errors (Fig. 9) are negligible by today's standards so the higher-order approximations are reserved for potential future use. For versions of FreeEOS prior to 1.5.0, the EOS1 option suite has employed the series described in Section 6 which suffered from a small discontinuity in EOS results (Fig. 9) which would sometimes interfere with the final stages of the Newton-Raphson iterations used in FreeEOS to find the solution.

FreeEOS is a free-energy based EOS so the result in the grand canonical partition function given by equation (21) requires a non-linear transformation to the equivalent free-energy exchange effect. I have developed an efficient numerical approximation for this transformation which should provide accurate results for both low degeneracy and high degeneracy with a smooth transition between the two limits.

The FreeEOS software library is licensed under the GPL and is freely downloadable from http://freeeos.sourceforge.net/.

I thank Forrest Rogers and Fritz Swenson for many useful discussions, drawing my attention to the importance of the exchange effect, and sharing the code for the Harwood approximation for $G(\eta)$; Santi Cassisi for providing representative model calculations and for his friendly encourage-

ment of my FreeEOS work; Ben Dorman and Don VandenBerg for helping to arouse my original interest in the EOS problem for stellar interiors; and Richard Stallman, Linus Torvalds, and many other programmers for the GNU/Linux computer operating system and accompanying tools that have made it practical to develop the FreeEOS code on personal computers. The figures of this paper have been generated with the PLplot (http://www.plplot.org) scientific plotting package.

REFERENCES

Anderson, E., Bai, Z., Bischof, C., Blackford, S., Demmel, J. Dongarra, J., Du Croz, J., Greenbaum, A., Hammarling, S., McKenney, A., & Sorensen, D. 1999, LAPACK Users' Guide, 3rd Ed. (Philadelphia: Society for Industrial and Applied Mathematics)

Basu, S., Christensen-Dalsgaard, J., Howe, R., Schou, J., Thompson, M. J., Hill, F., and Komm, R. 2003, ApJ, 591, 432

Cassisi, S. 2005, private communication

Cody, W. J., & Thacher, H. C. Jr. 1967, Math. Comp., 21, 30; erratum, 1967, Math. Comp., 21, 525

Cox, J. P., & Giuli, R. T. 1968, Principles of Stellar Structure (New York: Gordon and Breach) (CG)

DeWitt, H. E., 1969, in Low Luminosity Stars, ed. S. S. Kumar (New York: Gordon and Breach), p. 211

Dorman, B., Irwin, A. W., & Pedersen, B. B. 1991, ApJ, 381, 228

Eggleton, P. P., Faulkner, J., & Flannery B. P. 1973, A&A, 23, 325 (EFF)

Heckler, A. F. 1994, Phys. Rev. D, 49, 611

Irwin, A. W. 1987, A&A, 182, 348

Irwin, A. W. 2004a, http://freeeos.sourceforge.net/eff_fit.pdf (Paper I)

Irwin, A. W. 2004b, http://freeeos.sourceforge.net/solution.pdf (Paper II)

Irwin, A. W. 2005, http://freeeos.sourceforge.net/coulomb.pdf (Paper III)

Kapusta, J. I. 1989, Finite Temperature Field Theory (Cambridge: Cambridge University Press)

Kovetz, A., Lamb, D. Q., & Van Horn, H. M. 1972, ApJ, 174, 109 (KLVH)

Perrot, P., & Dharma-wardana, M. W. C. 1984, Phys. Rev. A, 30, 2619

Mihalas, D., Däppen, W., & Hummer, D. G. 1988, ApJ, 331, 815

Pietrinferni, A., Cassisi, S., Salaris, M., & Castelli, F. 2004, ApJ, 612, 168

Press, W. H., Flannery, B. P., Teukolsky, S. A., & Vetterling, W. T. 1986, Numerical Recipes (Cambridge, Cambridge University Press)

Rogers, F. J. 1986, ApJ, 310, 723

Rogers, F. J. & Nayfonov, A. 2002, ApJ, 576, 1064

Saumon, D., Chabrier, G., & Van Horn, H. M. 1995, ApJS, 99, 713

Stolzmann, W. & Blöcker, T. 1996, A&A314, 1024

Fig. 1.— A comparison of the loci of stellar-interior models as a function of the degeneracy parameter f and the relativity parameter g. The models (Cassisi 2005) were calculated for solar metallicity using the EOS1 option suite of FreeEOS and the stellar-evolution code that has been described in Pietrinferni, et al. (2004). The labels of '0.1", '0.3", '1.0", 'RGT", and 'CG" respectively indicate main-sequence models of 0.1, 0.3, and 1.0 $M_\odot$ and models of 1.0 $M_\odot$ evolved to the tip of the red-giant branch and to the initial clump-giant phase (zero-age horizontal branch of solar metallicity).

Fig. 2.— Differences of the $J^{\rm NR}$ integral as a function of the degeneracy parameter f. The differences are between equation 13 evaluated with the Harwood approximation to $G(\eta)$ and the non-relativistic limit of the J integral evaluated with precise numerical integration.

Fig. 3.— Differences of the $K^{\rm NR}$ integral as a function of the degeneracy parameter f. The differences are between equation 18 evaluated with the analytical derivative of the Cody-Thacher approximation and the non-relativistic limit of the K integral evaluated with precise numerical integration.

Fig. 4.— Differences of exchange integrals as a function of the degeneracy parameter f and the relativity parameter g. For both the J and K integrals, the differences are between series approximations as described in Section 6 and precise numerical integration.

Fig. 5.— Differences of exchange integrals as a function of the degeneracy parameter f and the relativity parameter g. The J-integral differences are between results calculated with equation (32) using coefficients from Tables 1 through 3 and results calculated with precise numerical integration. The K-integral differences are between results calculated with equation (37) using coefficients from Tables 4 through 6 and results calculated with precise numerical integration.

Fig. 6.— A comparison of EOS quantities and loci of model stellar interiors as a function of density and temperature at solar metallicity. The thin short-dashed line indicates where the radiative and gas pressures are equal, the boundary between the radiation-dominated and matter-dominated EOS. The thin dot-dashed line indicates where $\log g = 0$, the boundary between where the free electrons are non-relativistic and relativistic. The thin long-dashed line indicates where $\log f = 0$, the boundary between where the free electrons are non-degenerate and degenerate. The thin solid lines indicate the middle of important ionization and dissociation zones. The 'He^+", 'He", 'H", and 'H_2" labels respectively correspond to where half the helium is singly ionized or neutral and where half the hydrogen is in neutral monatomic form or in the diatomic molecular form. The medium thickness solid line indicates the current high-density, low-temperature calculation limit for FreeEOS (see text). The thick solid lines indicate the ρ, T loci of the same solar-metallicity model stellar interiors that were plotted in Figure 1. The labels of '0.1", '0.3", '1.0", 'RGT", and 'CG" respectively indicate main-sequence models of 0.1, 0.3, and 1.0 $M_\odot$ and models of 1.0 $M_\odot$ evolved to the tip of the red-giant branch and to the initial clump-giant phase (zero-age horizontal branch of solar metallicity).

Fig. 7.— Differences of pressure P and first adiabatic exponent Γ_1 as a function of the degeneracy parameter f and the relativity parameter g. In all cases the differences have been generated between comparison EOS calculations with the indicated modification to the EOS1 option suite and reference EOS calculations with the unmodified EOS1 option suite. For the "No exchange" differences the comparison calculations have been done with the EOS1 option suite modified to drop the exchange effect (see Sect. 6). For the "Linear exchange" differences the comparison calculations have been done with the the EOS1 option suite modified to use the linear-inversion approximation (see Sect. 6) to transform between $\ln Z_X$ and F_X. For the "Non-relativistic exchange" differences the comparison calculations have been done with the EOS1 option suite modified to replace equation (21) by equation (51), the non-relativistic limit of that equation.

Fig. 8.— The first adiabatic exponent Γ_1 and differences of first adiabatic exponent Γ_1, pressure P, and square of the sound speed, $v_s^2 = P\Gamma_1/\rho$ as a function of the (fixed) locus of ρ, T, and abundance points within a solar model. The differences are calculated identically to those of Figure 7. The 'No exchange" differences are indicated by solid lines, the 'Linear exchange" differences are indicated by short-dashed lines, and the 'Non-relativistic exchange" differences are indicated by long-dashed lines.

Fig. 9.— Differences of pressure P and first adiabatic exponent Γ_1 as a function of the degeneracy parameter f and the relativity parameter g. In all cases the differences have been generated between comparison EOS calculations with the indicated modification to the EOS1 option suite and reference EOS calculations with the EOS1 option suite modified to use the most accurate fits for the J and K integrals (i.e. the sixth-order fit for J and the seventh-order fit for K). For the "Series exchange" differences the comparison calculations have been done with the EOS1 option suite modified to use the series approximations for J and K discussed in Section 6. For the 'Second-order exchange approximation" differences the comparison calculations have been done with the unmodified EOS1 option suite (i.e., using the second-order fits for J and K).

Table 1: Second-order fitting coefficients for J

m	$\widehat{J}_{m,0}$	$\widehat{J}_{m,1}$	$\widehat{J}_{m,2}$
0	34.8358213	6.1265167	0.8600275
1	86.1918396	25.7316016	5.6471122
2	51.5419186	29.3774454	7.0535536
m	$\widehat{J'}_{m,0}$	$\widehat{J'}_{m,1}$	$\widehat{J'}_{m,2}$
0	33.2562696	31.5537757	6.8170355
1	66.7030494	65.6524569	14.8834241
2	28.4278181	30.6499630	8.0074649
m	$\widehat{J''}_{m,0}$	$\widehat{J''}_{m,1}$	$\widehat{J''}_{m,2}$
0	7.6128464	2.7809264	2.4421025
1	16.9077576	8.2810716	6.7537105
2	7.1078540	9.0118836	1.1701926

Note. — This fit has $M = N = M' = N' = M'' = N'' = 2$ and a maximum relative fitting error of $10^{-2.3}$.

Table 2: Fourth-order fitting coefficients for J

m	$\widehat{J}_{m,0}$	$\widehat{J}_{m,1}$	$\widehat{J}_{m,2}$		
0	56.2805336	1.4600744	0.8040612		
1	155.6222406	-38.3239264	10.8897054		
2	83.5532182	28.8234751	7.0883559		
m	$\widehat{J'}_{m,0}$	$\widehat{J'}_{m,1}$	$\widehat{J'}_{m,2}$	$\widehat{J'}_{m,3}$	$\widehat{J'}_{m,4}$
0	5.6437776	72.0785970	105.3785812	46.7695962	6.8234346
1	174.7225632	700.7413357	598.6273693	198.3020460	28.4677241
2	1174.0556985	1553.6277210	854.7360263	291.6944973	43.6666247
3	69.7350999	461.3841453	494.9380271	200.3802976	31.6890797
4	-19.1101716	32.3236302	87.5200915	47.0467342	8.0006636
m	$\widehat{J''}_{m,0}$	$\widehat{J''}_{m,1}$	$\widehat{J''}_{m,2}$	$\widehat{J''}_{m,3}$	$\widehat{J''}_{m,4}$
0	28.6410004	165.6488584	274.3616284	-7.8112104	7.6299746
1	108.8331950	1460.9695944	848.1550036	-24.4941518	23.9006008
2	144.3375035	2059.8613336	932.1227056	-37.9448618	32.1617806
3	94.8689197	649.1216512	513.4043189	-49.7713793	31.8665472
4	15.7800513	43.7140906	40.9849434	10.9901399	3.4726043

Note. — This fit has $M = N = 2$, $M' = N' = M'' = N'' = 4$, and a maximum relative fitting error of $10^{-3.1}$.

Table 3: Sixth-order fitting coefficients for J

m	$\widehat{J}_{m,0}$	$\widehat{J}_{m,1}$	$\widehat{J}_{m,2}$	$\widehat{J}_{m,3}$
0	77.7223322	15.1130448	-2.6865083	0.7914812
1	329.9690751	-1711.5422468	1199.9753651	-73.9603649
2	339.1739022	778.5679695	54.6086181	14.3235218
3	115.5562291	74.2173982	31.4786125	7.0902001
m	$\widehat{J'}_{m,0}$	$\widehat{J'}_{m,1}$	$\widehat{J'}_{m,2}$	$\widehat{J'}_{m,3}$
	$\widehat{J'}_{m,4}$	$\widehat{J'}_{m,5}$	$\widehat{J'}_{m,6}$	
0	-5.4000121	146.7136763	411.6203402	441.1299352
	232.4649446	61.5101678	6.8247249	
1	5695.7957148	-7092.1165083	-13101.9904352	-2447.2072200
	1014.6845310	368.7097096	42.0150160	
2	11216.4052787	28977.5973434	27389.3394169	13360.4808816
	4202.0496258	953.5922014	107.4877403	
3	-5004.0576957	-17432.3188130	-4881.7422341	7561.9107837
	4667.0296065	1274.5396464	149.2296305	
4	-2978.6276336	-6011.6709017	-4714.8750809	776.1294503
	2627.0527294	942.4763969	113.1130650	
5	-990.8463971	-1902.4091931	-1278.8279881	974.1793642
	1238.7406226	392.2869249	48.0123563	
6	-61.0768342	-3.5689832	243.7667578	349.9756271
	213.4913981	63.9909089	8.0000291	
m	$\widehat{J''}_{m,0}$	$\widehat{J''}_{m,1}$	$\widehat{J''}_{m,2}$	$\widehat{J''}_{m,3}$
	$\widehat{J''}_{m,4}$	$\widehat{J''}_{m,5}$	$\widehat{J''}_{m,6}$	
0	76.9669717	4196.5960409	-14690.7086472	-11483.9761233
	273.9069680	925.7506712	-78.6975448	
1	403.8465365	13947.6028263	-10481.5778168	-8157.4031117
	7797.1164005	4392.2634040	-351.4769520	
2	877.1286674	6386.7560942	-10134.5858478	4139.5945610
	19163.2886021	7721.2581060	-595.0931958	
3	1009.2265882	-8509.1033779	-31981.8034156	-2456.0463932
	15475.1207915	6649.2247613	-468.7739531	
4	625.3080827	-5068.4236377	-14050.4153207	-4921.9776737
	5080.5195211	2808.9762429	-177.7836871	
5	215.1119554	-116.6120752	220.8791890	-980.5436208
	1423.8520116	365.3071337	4.6112748	
6	23.7703342	60.5395737	138.3380767	49.8463981
	107.3457476	20.1232319	3.3403911	

Note. — This fit has $M = N = 3$, $M' = N' = M'' = N'' = 6$, and a maximum relative fitting error of $10^{-4.1}$.

Table 4: Second-order fitting coefficients for K

m	$\widehat{K}_{m,0}$	$\widehat{K}_{m,1}$	$\widehat{K}_{m,2}$
0	9.4150106	9.0399638	2.6135398
1	19.3949179	18.4548660	5.2690297
2	10.5602307	9.8746980	2.8270724
m	$\widehat{K'}_{m,0}$		
0	0.2219891		

Note. — This fit has $M = N = 2$, $M' = N' = 0$, and a maximum relative fitting error of $10^{-2.5}$.

Table 5: Fourth-order fitting coefficients for K

m	$\widehat{K}_{m,0}$	$\widehat{K}_{m,1}$	$\widehat{K}_{m,2}$	$\widehat{K}_{m,3}$	$\widehat{K}_{m,4}$
0	15.9616640	31.6264744	30.8574217	14.3505923	2.6124722
1	65.2137462	128.5287114	124.7941936	58.0368244	10.5422097
2	100.0779497	196.2665661	189.7875295	88.3645023	16.0646752
3	68.9805226	134.3128503	128.9954761	59.8503499	10.8120877
4	18.1027203	35.0222537	33.5069500	15.5482948	2.8284087
m	$\widehat{K'}_{m,0}$				
0	0.7085843				
1	0.4384647				

Note. — This fit has $M = N = 4$, $M' = 1$, $N' = 0$, and a maximum relative fitting error of $10^{-3.8}$.

Table 6: Seventh-order fitting coefficients for K

m	$\widehat{K}_{m,0}$	$\widehat{K}_{m,1}$	$\widehat{K}_{m,2}$	$\widehat{K}_{m,3}$
	$\widehat{K}_{m,4}$	$\widehat{K}_{m,5}$	$\widehat{K}_{m,6}$	$\widehat{K}_{m,7}$
0	25.7842747	89.6532756	178.2531213	220.2391122
	171.7202945	82.5677241	22.2022652	2.6124292
1	182.7491698	634.2399245	1258.5795649	1552.0338194
	1209.2423616	580.9794546	156.3493557	18.3854785
2	556.4181655	1927.2484177	3816.1015364	4696.8562020
	3655.4138590	1754.9056233	472.5034538	55.5290929
3	938.5331301	3244.9585385	6413.7471264	7879.1826389
	6129.2942522	2940.4105339	792.5785975	93.0966512
4	960.7519007	3313.2266232	6532.0560019	8002.6234013
	6214.1077832	2977.6103202	802.1268594	94.1489718
5	583.5117994	2009.3901546	3952.7213124	4839.3366977
	3753.8298340	1798.9814958	485.3881563	56.9861334
6	200.4860761	688.3557251	1350.3664972	1647.8294240
	1275.4438080	610.3316895	164.4720854	19.2907139
7	29.4157259	100.8001430	197.3155508	240.4593766
	185.9307018	89.0447118	24.0404251	2.8284359

m	$\widehat{K'}_{m,0}$
0	1.0175489
1	0.5914964

Note. — This fit has $M = N = 7$, $M' = 1$, $N' = 0$, and a maximum relative fitting error of $10^{-4.6}$.

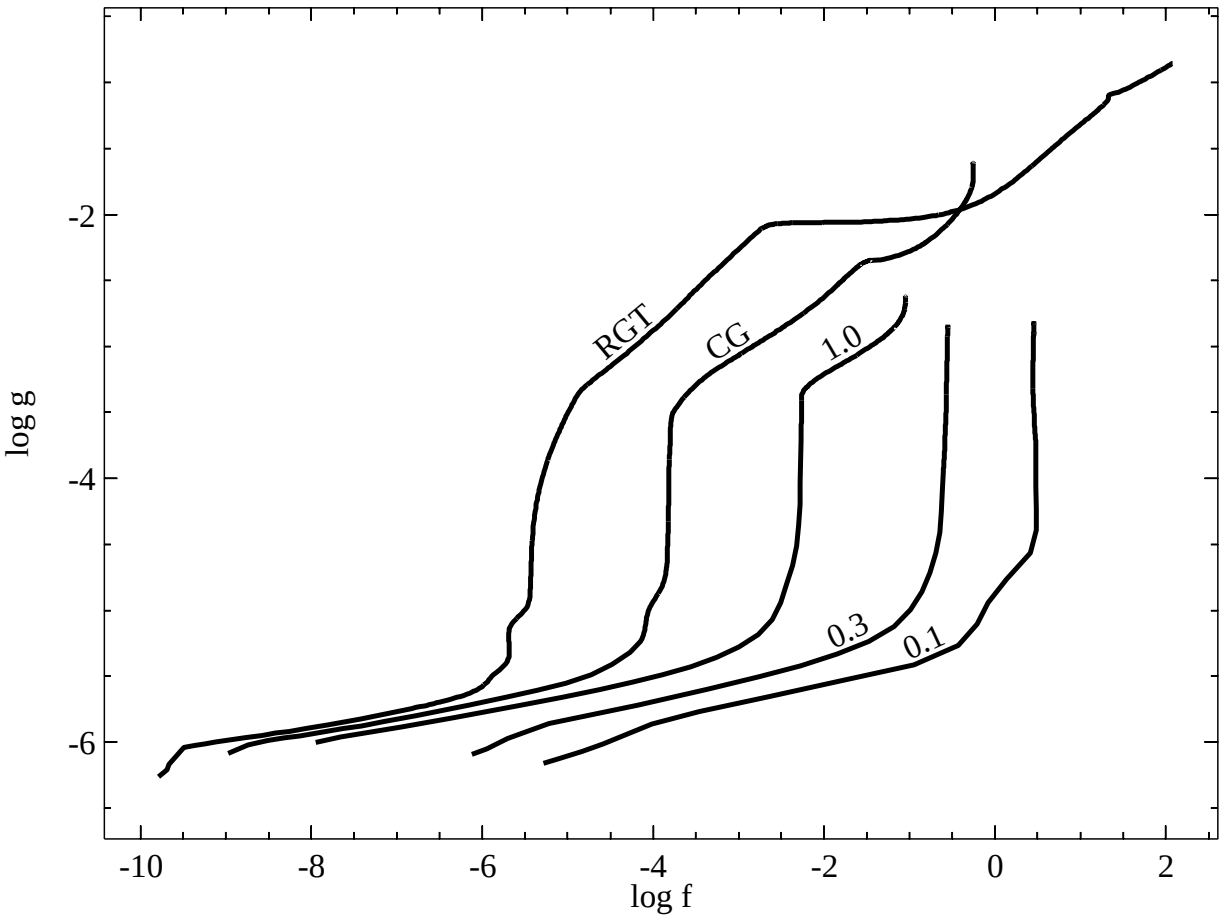
log g
-2
-4
-6
-10
-8
-6
-4
-2
0
2
log f
RGT
CG
1.0
0.3
0.1

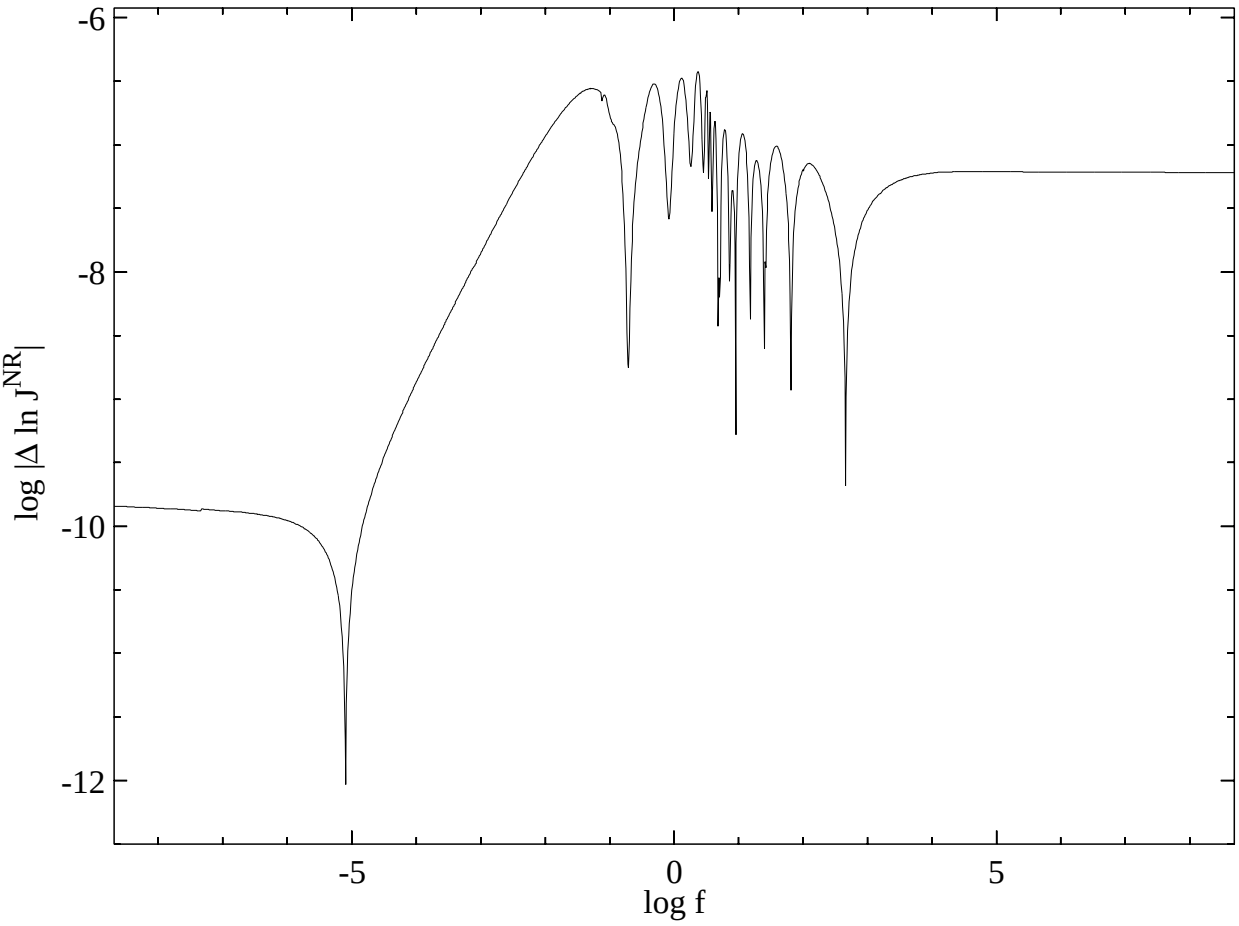
-6
-8
-10
-12
log |Δ ln J^NR|
-5
0
5
log f

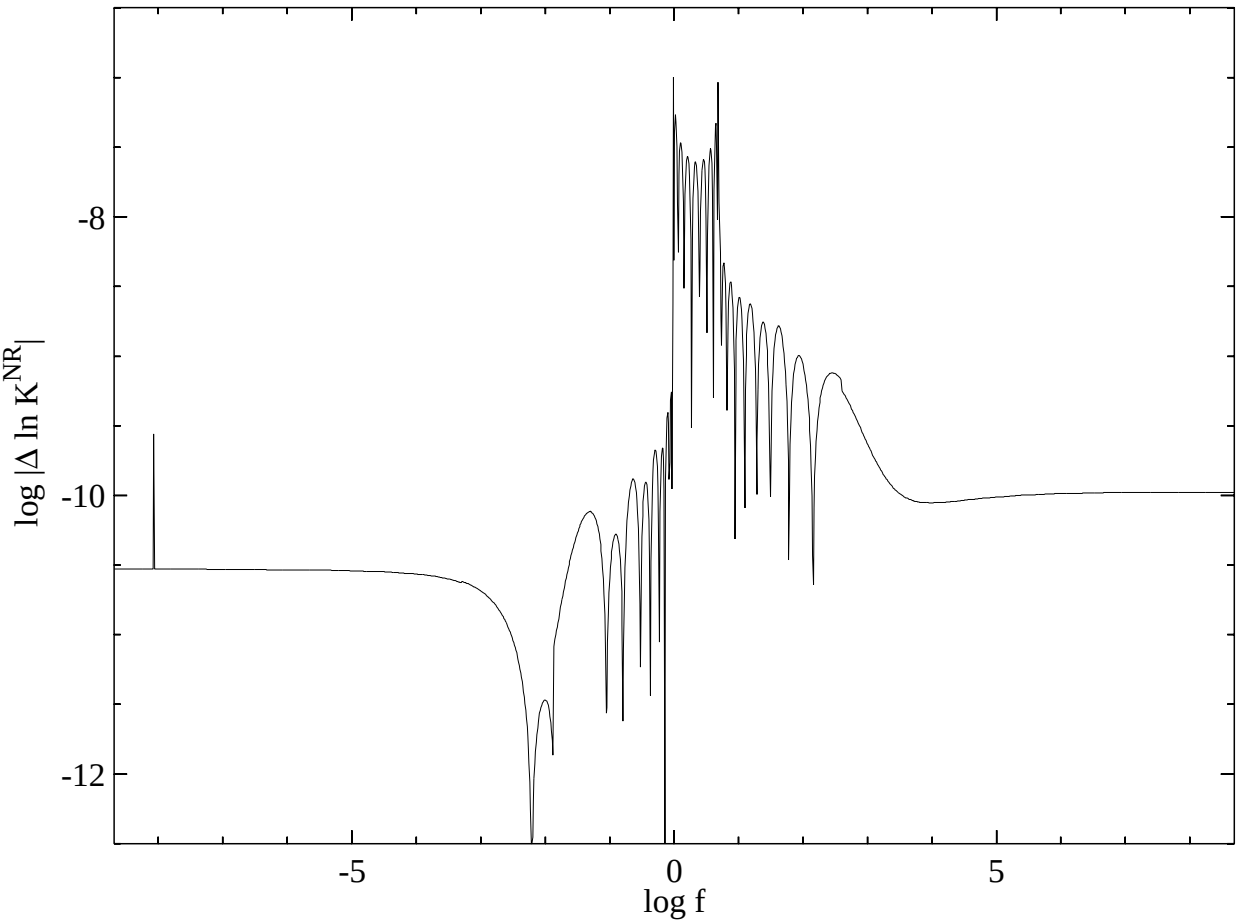
log |Δ ln K^NR|
-8
-10
-12
-5
0
5
log f

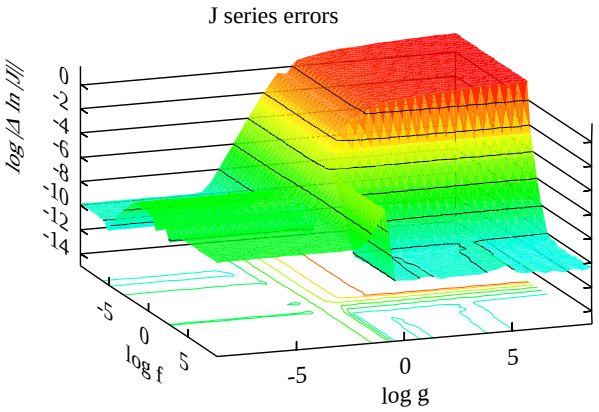
J series errors
log |Δ ln J|
-5
0
5
log f
-5
0
5
log g

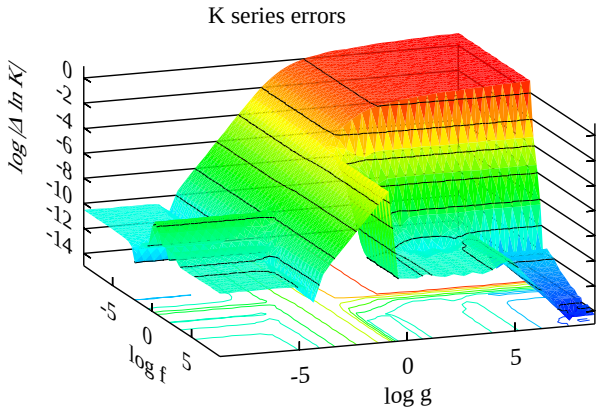
K series errors
log |Δ ln K|
-5
0
5
log f
-5
0
5
log g

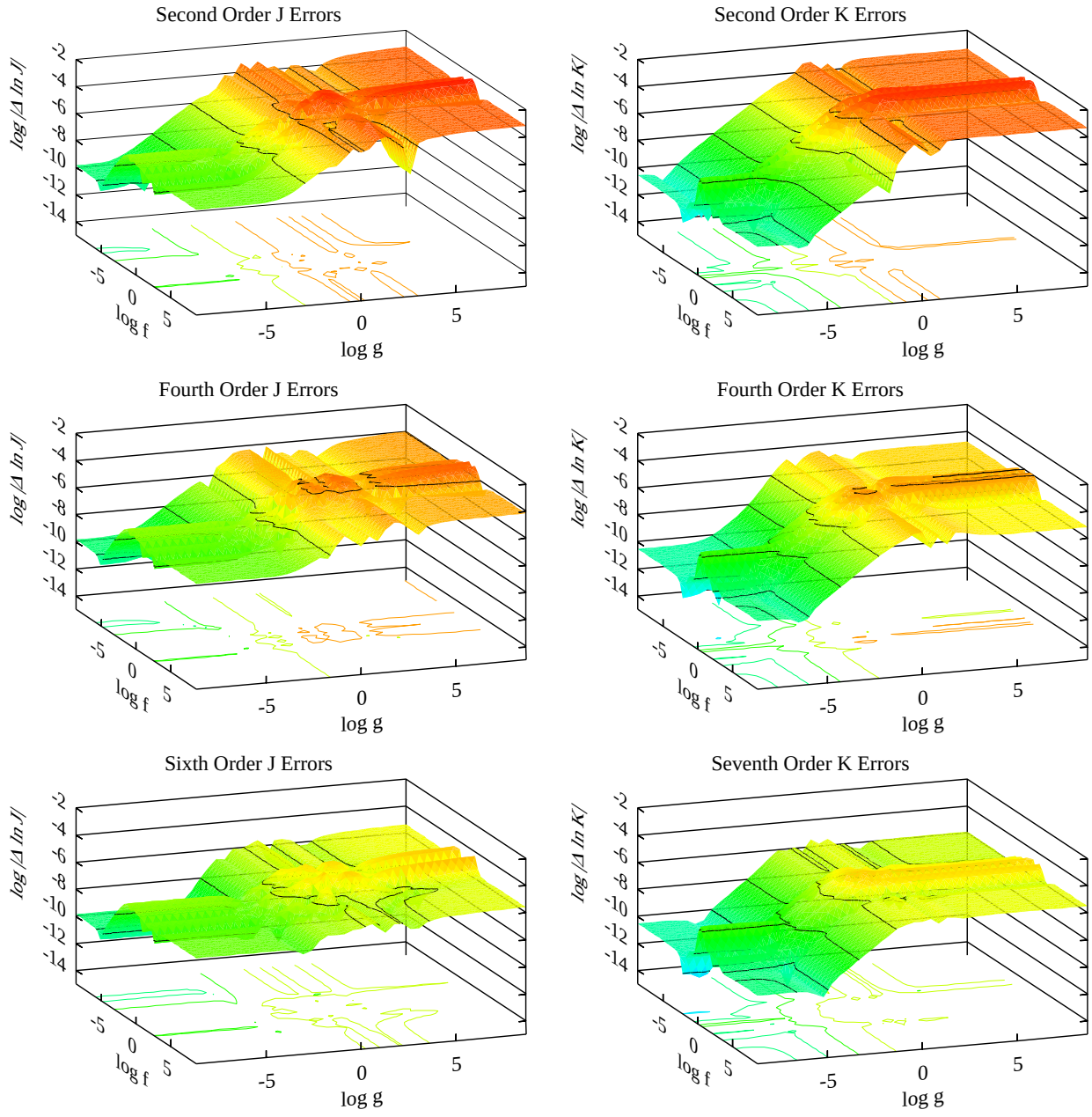
Second Order J Errors
log |Δ ln J|
-2
-4
-6
-8
-10
-12
-14
log f
5
0
-5
log g
-5
0
5
Second Order K Errors
log |Δ ln K|
Fourth Order J Errors
Fourth Order K Errors
Sixth Order J Errors
Seventh Order K Errors

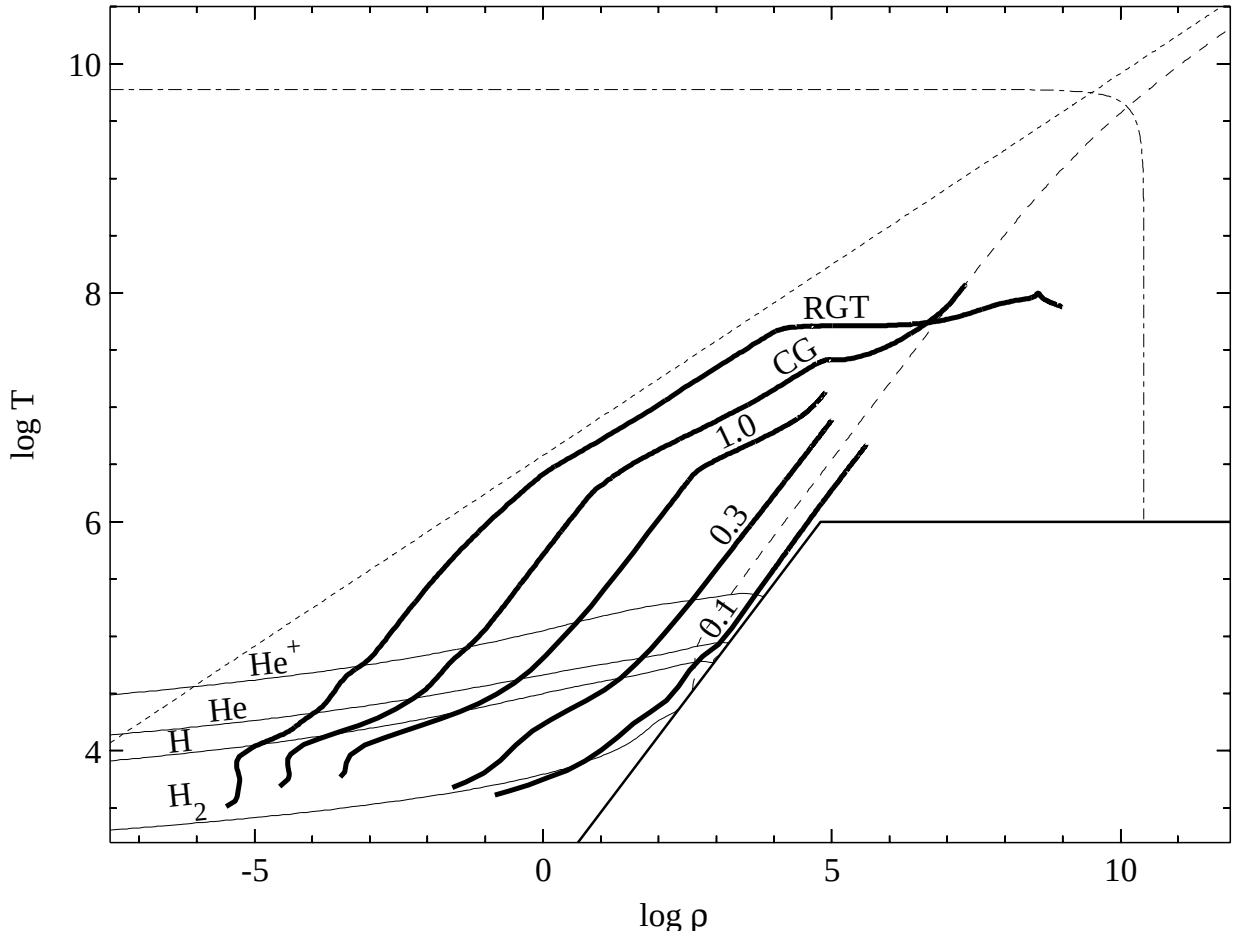
10
8
6
4
log T
-5
0
5
10
log ρ
RGT
CG
1.0
0.3
0.1
He+
He
H
H2

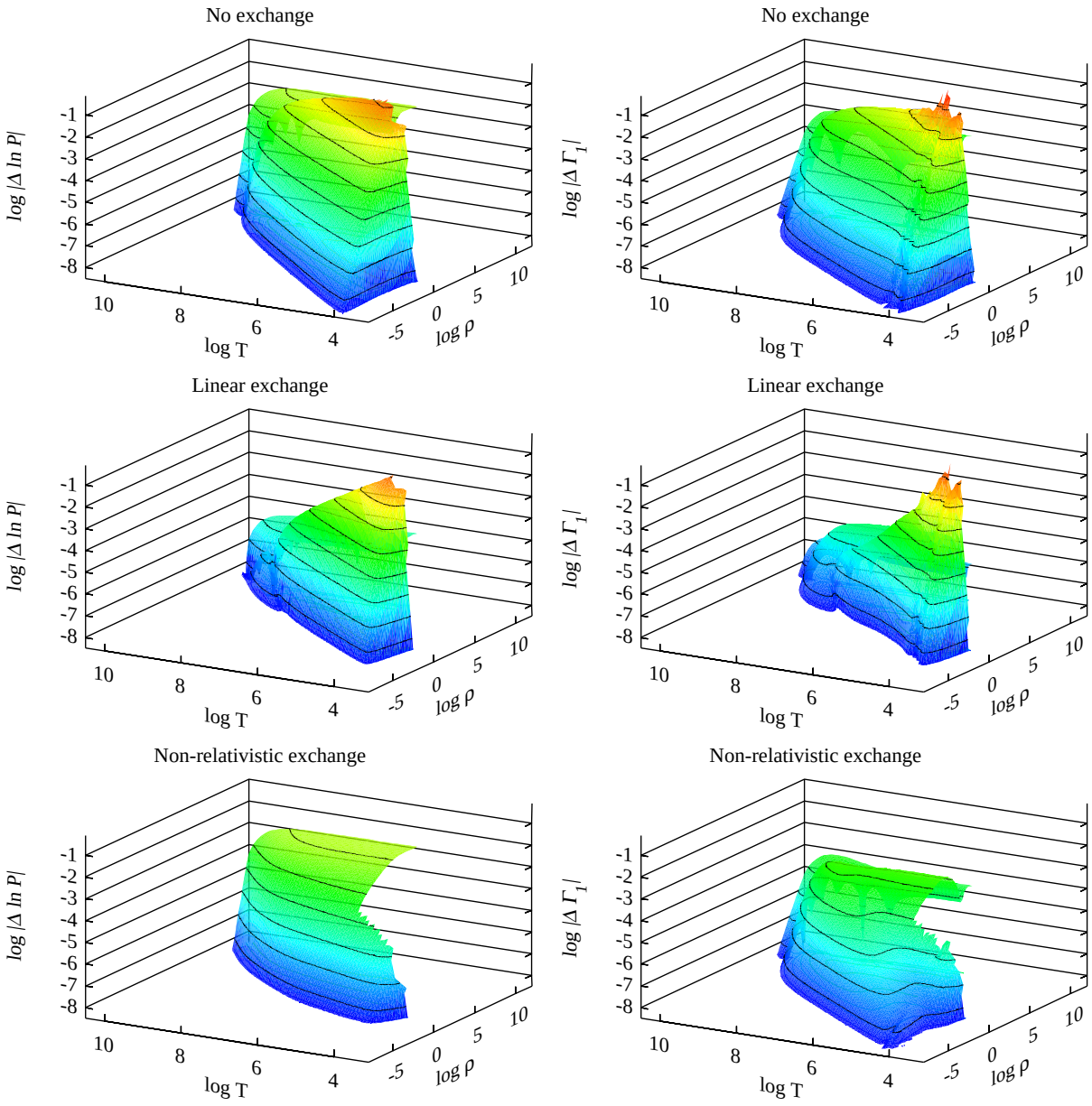
No exchange
No exchange
Linear exchange
Linear exchange
Non-relativistic exchange
Non-relativistic exchange
log |Δ ln P|
log |Δ Γ1|
log T
log ρ
-1
-2
-3
-4
-5
-6
-7
-8
10
8
6
4
-5
0
5
10

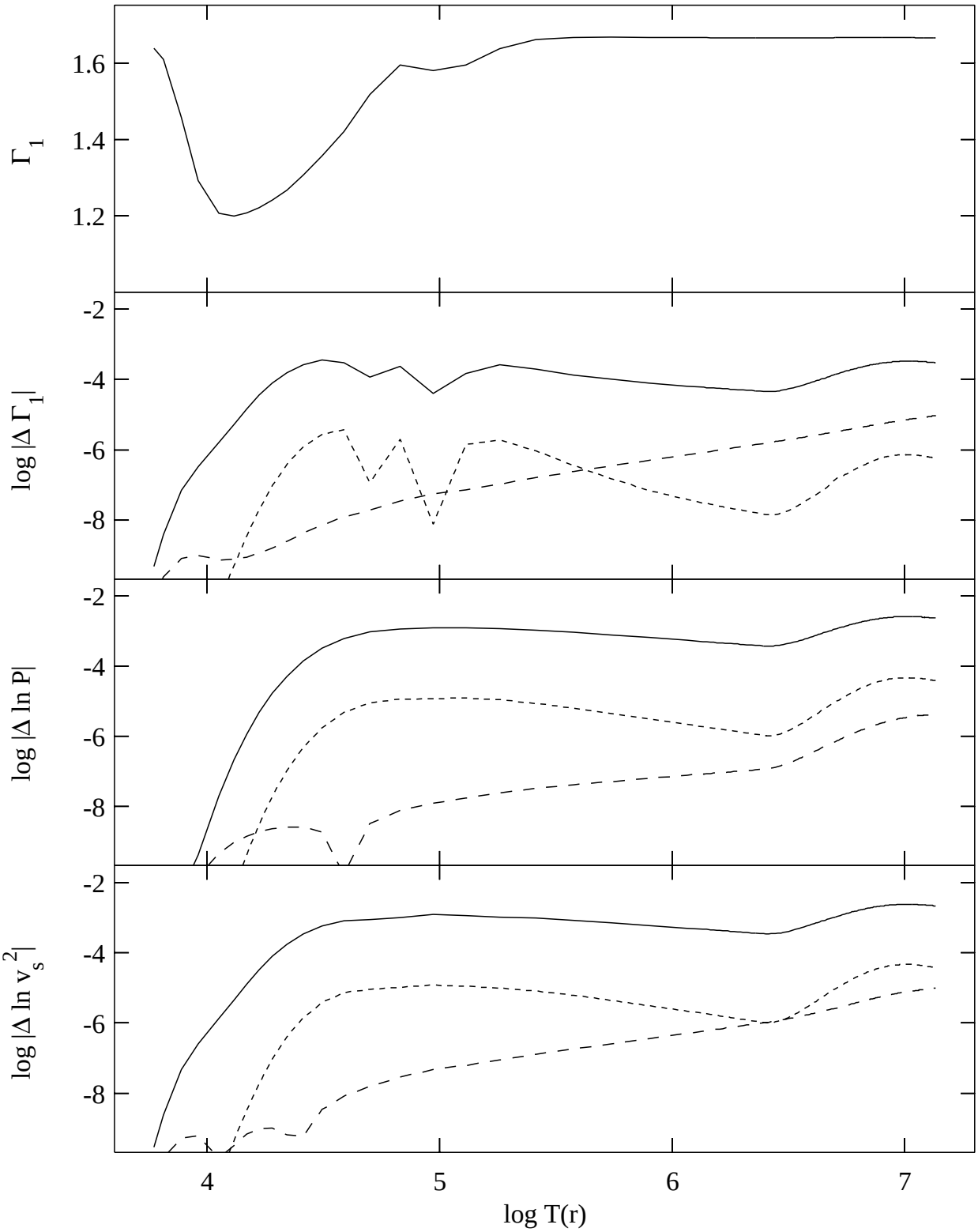
Γ1
1.6
1.4
1.2
log |Δ Γ1|
-2
-4
-6
-8
log |Δ ln P|
-2
-4
-6
-8
log |Δ ln vs2|
-2
-4
-6
-8
4
5
6
7
log T(r)

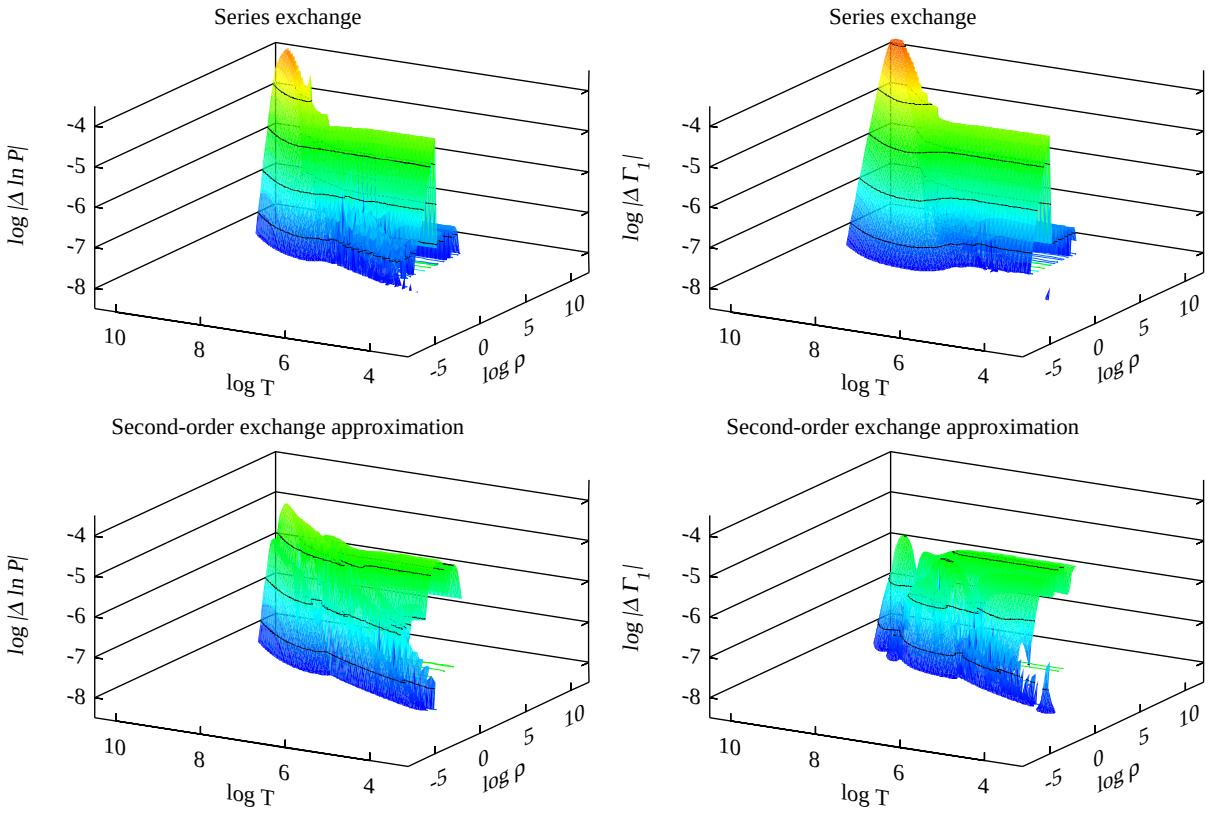
Series exchange
log |Δ ln P|
-4
-5
-6
-7
-8
10
8
6
4
log T
-5
0
5
10
log ρ
Series exchange
log |Δ Γ1|
-4
-5
-6
-7
-8
10
8
6
4
log T
-5
0
5
10
log ρ
Second-order exchange approximation
log |Δ ln P|
-4
-5
-6
-7
-8
10
8
6
4
log T
-5
0
5
10
log ρ
Second-order exchange approximation
log |Δ Γ1|
-4
-5
-6
-7
-8
10
8
6
4
log T
-5
0
5
10
log ρ